Sensors and Actuators A 171 (2011) 55–62

Contents lists available at ScienceDirect

Sensors and Actuators A: Physical

journal homepage: www.elsevier.com/locate/sna

# Detection of microdroplet size and speed using capacitive sensors

Caglar Elbuken, Tomasz Glawdel, Danny Chan, Carolyn L. Ren*

*Department of Mechanical and Mechatronics Engineering, University of Waterloo, 200 University Ave W., Waterloo, ON, Canada N2L 3G1*

ARTICLE INFO

*Article history:*
Received 18 March 2011
Received in revised form 21 June 2011
Accepted 13 July 2011
Available online 23 July 2011

*Keywords:*
Microdroplet detection
Two-phase flow
Microfluidics
Capacitive sensor
Coplanar electrodes

ABSTRACT

Detection of the presence, size and speed of microdroplets in microfluidic devices is presented using commercially available capacitive sensors which make the droplet based microfluidic systems scalable and inexpensive. Cross-contamination between the droplets is eliminated by introducing a passivation layer between the sensing electrodes and droplets. A simple T-junction generator is used to generate droplets in microchannels. Coplanar electrodes are used to form a capacitance through the microfluidic channel. The change in capacitance due to the presence of a droplet in the sensing area is detected and used to determine the size and speed of the droplet. The design of a single pair of electrodes is used to detect the presence of a droplet and the interdigital finger design is used to detect the size and speed of the droplet. An analytical model is developed to predict the detection signal and guide the experimental optimization of the sensor geometry. The measured droplet information is displayed through a Labview interface in real-time. The use of capacitance sensors to monitor droplet sorting at a T-junction is also presented. The discussions in this paper can be generalized to any droplet detection application and can serve as a guideline in sensor selection.



## 1. Introduction

Recently, significant attention has been given to the development of droplet based microfluidic devices due to their potential in high throughput applications such as biochemical screening [1–3], particle synthesis [4–6] and chemical analysis [7]. A fundamental challenge in designing these devices is managing droplet traffic within large scale networks [8]. Droplets alter the hydrodynamic resistance of microchannels which causes varying global flow fields throughout the network as droplets move in and out of channels. This leads to complex droplet movement even in the most basic configurations such as a single T-junction bifurcation [9–13]. Controlling droplet traffic therefore requires real-time detection and manipulation of droplets in multiple locations. Furthermore, in systems that include merging and breakup elements, detecting droplet size and speed is equally important [14]. In this study, we present a cost effective sensor design that uses capacitance change to measure droplet presence, size and speed.

The two most common means of droplet detection are optical and electrical sensing. The majority of the proof-of-concept devices use a microscope and high speed camera to monitor droplets. For simple devices that require a few sensors, optical droplet detectors can be implemented by integrating a light source and detector aligned with the channels [15,16]. Although these systems achieve droplet detection at kHz range, the bulky and expensive off-chip components limit the use of optical techniques for complicated devices. On the other hand, electrical sensing provides a scalable, low power and cost-effective alternative to optical methods. Electrical detection of microdroplets may be considered as a simpler version of cellular impedance spectroscopy which uses both the resistive and capacitive components of the detection signal to retrieve information such as size of particles, viability of cells, membrane properties and subcellular content [17–19]. Droplets can be detected in a similar manner because of the stark contrast in the electrical properties of the two phases (oil and aqueous). Generally, the conductivity and permitivity of the aqueous dispersed phase is significantly higher than the oil based continuous phase, which makes electrical sensing an ideal candidate for droplet detection.

Early studies demonstrated droplet detection via resistive changes using coplanar electrodes [20–23]. The major limitation of resistive sensing is that it requires a conductive continuous phase to reflect a change associated with the presence of droplets in the sensing area [22]. However, when droplets are non-wetting and a thin-film of oil separates the droplet from the electrodes, the change in resistance is too low to be detected with conventional detection circuits. Wetting should be avoided in most applications since it leads to cross-contamination between droplets which limits the use of resistive detection for droplet based microfluidic devices. Alternatively, capacitive detection can detect droplets without any contact between the droplet and electrode surface. When a droplet enters the sensing area, changing dielectric constant yields a change in capacitance between the electrodes. Previously,

* Corresponding author. Tel.: +1 519 888 4567x33030; fax: +1 519 885 5862.
*E-mail address:* c3ren@uwaterloo.ca (C.L. Ren).

0924-4247/$ – see front matter © 2011 Elsevier B.V. All rights reserved.
doi:10.1016/j.sna.2011.07.007

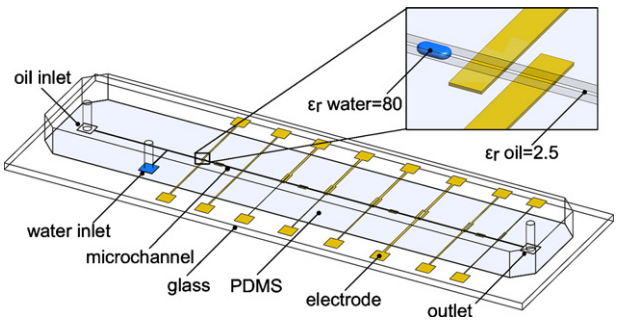


**Fig. 1.** Schematic of the microfluidic chip with T-junction droplet generator and coplanar electrodes placed beneath the microchannel forming the capacitive sensors. A single channel passes over several electrode designs with different electrode gaps and widths.

capacitive droplet detection has been shown using complex circuitries such as relaxation oscillators and sigma-delta modulators that are out of the reach of most microfluidic designers [24–28]. One of the biggest hurdles in the applicability of droplet based approaches is the lack of standardized tools and instruments that enable the development of robust platforms with high reproducibility. Aside from developing innovative tools and functions for microfluidic systems, it is equally important to make these systems easily available for researchers from different disciplines. This study aims to fill this gap by presenting a microdroplet size and speed detection method using commercially available and inexpensive capacitance sensors.

In this study, we use well-developed, robust fabrication procedures and off-the-shelf components to achieve scalable and cost-effective detection of droplet size and speed. This approach is in parallel to some other applications of commercial capacitance sensors such as MEMS accelerometer and capacitive coulter counting [29,30]. We used coplanar electrodes to form a capacitance through the microchannel. A passivation layer is introduced to prevent direct contact between the electrodes and droplet. In order to serve as a guideline in sensor design, an analytical model is developed taking into account the effect of passivation layer. In addition, detection of droplet size and speed is demonstrated using the design of interdigital electrodes. The detection limit and scalability of the sensors are also discussed.

## 2. Sensor design

Capacitive sensing of microdroplets is based on the contrast of dielectric property between the dispersed and continuous phase. Typically water ($\varepsilon_r = 80$) and oil ($\varepsilon_r = 2.5$) are the two phases which results in a 32-fold difference in dielectric constant between the two phases. Microbubbles may also be detected if the contrast of dielectric property between the liquid and gas phases is large. In this study, droplets are detected with coplanar electrodes placed beneath the microchannel as shown in Fig. 1. Several electrode designs were tested that varied in the size, spacing and number of electrode fingers.

Maximizing the detection signal requires an effective sensor design. Capacitance sensors based on a single pair of fingers or interdigital (i.e. combed) fingers have been studied extensively for a number of applications [31]. Chen et al. previously analyzed detection of droplets using planar capacitance sensors assuming that the droplets are in contact with the electrodes [24]. However, our design includes a thin passivation layer to prevent cross contamination. Our preliminary experiments revealed that the thickness of the passivation layer strongly affects the signal strength. When developing an analytical model of the detection we take into account the influence of the passivation layer. Our analytical model

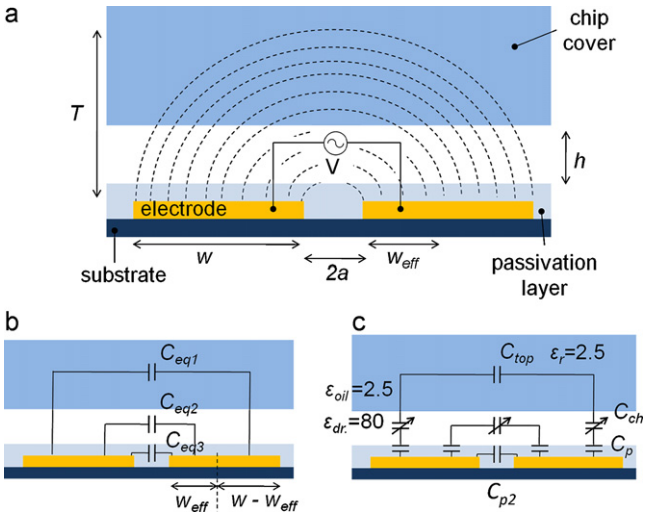


**Fig. 2.** Illustration of field lines/capacitances formed by coplanar electrodes placed beneath a microchannel. (a) Field lines between the electrodes, (b) parallel equivalent capacitances, (c) individual capacitances formed through the passivation layer ($C_p$), channel ($C_{ch}$) and chip cover ($C_{top}$).

is based on the analysis presented by Chen et al. Applying conformal mapping techniques, Chen et al. showed that the capacitance created by a pair of coplanar electrodes in a semi-infinite domain is given as [24]

$$C = \frac{2 \in_r \in_0 l}{\pi} \ln\left[1 + \frac{w}{a} + \sqrt{\left(1 + \frac{w}{a}\right)^2 - 1}\right] \quad (1)$$

where $\varepsilon_r$ is the dielectric constant, $\varepsilon_0$ is the electric constant, $l$ is the length of the electrodes (into the paper), $w$ is the width of the electrodes and $a$ is the half-gap between the electrodes (Fig. 2(a)). Although this equation is derived assuming $w/a \gg 1$, it is still a good approximation when $w \approx a$. For $w/a = 1.1$, for instance, Eq. (1) approximates the capacitance within 10% error [24].

The width of the electrodes and the spacing between them determine the penetration depth ($T$) of the field lines. When coplanar electrodes are placed beneath a microchannel, some field lines may go through the chip cover as shown in Fig. 2(a).

If the cover material has a dielectric constant much lower than the channel, field lines passing through the cover do not contribute to the change in capacitance detected by the sensor. This causes only a portion of the electrode to be active, which is defined as the effective width ($w_{eff}$) of the electrode [24]

$$W_{eff} = a\left(\sqrt{1 + \left(\frac{h}{a}\right)^2} - 1\right) \quad (2)$$

The effective width for $h = 50\ \mu m$ and $a = 10\ \mu m$ is calculated as $w_{eff} = 41\ \mu m$. Assuming the cover has a negligible dielectric constant compared to the channel, it implies that electrodes wider than 41 μm will produce the same capacitance. This represents the maximum effective size of the electrodes.

In our design the change in capacitance must be calculated while also considering the effect of the passivation layer. The total semi-infinite capacitance formed by a pair of coplanar electrodes beneath a microchannel with a passivation layer can be written as

$$C_T = C_{eq1} + C_{eq2} + C_{eq3} \quad (3)$$

where $C_{eq1}$, $C_{eq2}$, $C_{eq3}$ are parallel equivalent capacitances formed through different field line paths between the electrodes as shown in Fig. 2(b). Denoting the capacitance over the channel as $C_{ch}$, the

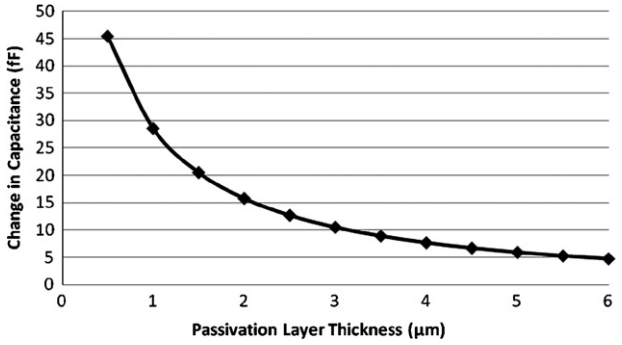


**Fig. 3.** Analytical results of change in capacitance for coplanar electrodes ($2a = 20\,\mu m$, $h = 50\,\mu m$, $w_{eff} = 41\,\mu m$, and $l = 100\,\mu m$).

passivation layer as $C_p$ and the top of the channel as $C_{top}$, the equivalent capacitances in Eq. (3) can be written as (Fig. 3(c))

$$C_{eq1} = \frac{C_p \cdot C_{ch} \cdot C_{top}}{C_p \cdot C_{ch} + 2C_{top}(C_p + C_{ch})} \tag{4}$$

$$C_{eq2} = \frac{C_p/2 \cdot C_{ch}}{C_p/2 + C_{ch}} = \frac{C_p \cdot C_{ch}}{C_p + 2C_{ch}}$$
$$C_{eq3} = C_{p2}$$

The double layer capacitance is considered as part of the passivation layer capacitance. The change in capacitance due to droplets moving in the channel is then

$$\Delta C_T = \Delta C_{eq1} + \Delta C_{eq2} + \Delta C_{eq3} \approx \Delta C_{eq2} \tag{5}$$

In the above equation $C_{eq1}$ has negligible effects on the change in capacitance due to very low $C_{top}$ that remains constant. $C_{eq1}$ is formed by the portion of the electrode larger than the $w_{eff}$ (Fig. 2(b)). Since $C_{p2}$ is also constant, the detection signal can be approximated as

$$\Delta C_T \approx \Delta C_{eq2} = \Delta \frac{C_p \cdot C_{ch}}{C_p + 2C_{ch}} = \Delta \frac{C_{ch}}{1 + 2(C_{ch}/C_p)} \tag{6}$$

where $C_p = \varepsilon A/t_p$ ($A$ – area of electrode top surface, $t_p$ – passivation layer thickness) and $C_{ch}$ is calculated by Eq. (1). In this study, the thickness of the passivation layer is less than 2 μm therefore the geometric assumption used to develop Eq. (1) is still valid for calculating $C_{ch}$. From Eq. (6), it can be seen that in order to increase the detection signal, $\Delta C_T$ the thickness of the passivation layer should be decreased. In Fig. 3, $\Delta C_T$ is plotted as a function of $t_p$ for water ($\varepsilon_r = 80$) in oil ($\varepsilon_r = 2.5$) droplet system with planar electrodes of 20 μm spacing. The PDMS ($\varepsilon_r = 2.5$) microchannel height and width are 50 μm and 100 μm, respectively. It is seen that passivation layer thickness changes the detection signal nonlinearly. The thinner the passivation layer, the higher the detected signal. However, fabrication of a very thin, uniform passivation layer is very challenging. This is a limiting factor for the minimum thickness of passivation layer that can be produced reliably. The sensitivity of the commercial capacitor sensors should also be taken into account when determining the passivation layer thickness. Using a very thick passivation layer may decrease the change in capacitance below the detection limit of the sensor.

## 3. Fabrication and experimental setup

Fabricating microfluidic chips integrated with capacitance sensors is a two step process involving the fabrication of the electrodes using lift-off and the PDMS microchannel using standard soft lithography techniques [32]. To make the electrodes, hexamethyldisiloxane (HMDS) was first spin-coated on a standard microscope slide at 3000 rpm for 60 s, which was followed by spin-coating positive photoresist (Microposit S1813) at 3000 rpm for 60 s. Next the photoresist was baked at 150 °C for 1.5 min and then exposed to UV-light (365 nm) through a transparency mask (CAD/Art Services) containing the electrode designs which was followed by development in Microposit MF-319 for 2 min. Then, 100 Å Cr/1000 Å Cu/100 Å Cr was deposited using magnetron sputtering (AJA Orion5). Fabrication of electrodes was completed with lift-off in Microposit Remover 1165 at 65 °C under ultrasonic agitation.

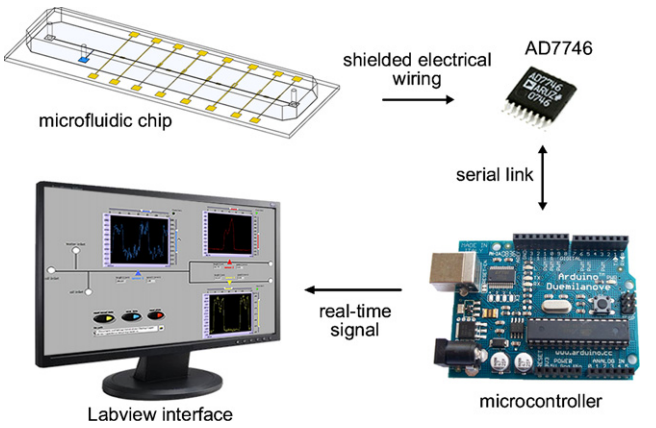


**Fig. 4.** Schematic of capacitive droplet detection system. Connection to the microfluidic chip is made via shielded ribbon cables and gold spring-pins. The AD7746 communicates with the microcontroller using the I2C protocol. The data is sent to the computer over a standard USB connection and displayed through a Labview interface.

Microchannels were fabricated from polydimethylsiloxane (PDMS) using standard soft lithography techniques. The thinner the passivation layer, the higher the sensor sensitivity, however this must be balanced by the need to keep droplets from contacting electrodes. Throughout this study, a 2 μm-thick passivation layer is used. To achieve a uniform 2 μm-thick coating, PDMS thinned with toluene (1:3 (w/w) PDMS/toluene) was spin-coated at 4000 rpm for 60 s followed by 1hr curing at 90 °C [33]. The complete chip was formed by bonding the microscope slide containing the electrodes on its surface with the PDMS substrate containing the microchannel using $O_2$ plasma (Harrick Plasma) at 500 mTorr, 29.6 W for 30 s. To achieve the right wetting conditions for silicone oil, the chip was then baked at 200 °C for 12 h.

Fluids were controlled using a microfluidic pressure controller system (Fluigent MFCS-8C). Water in silicone oil (10 mPa s) droplets were formed using a T-junction generator [34]. For a given geometry, the size and speed of the droplets can be controlled by adjusting the pressure to the two inlets. Plug-like droplets where the length of the droplet is larger than its width were created in this study. A high speed camera (Phantom v210, Vision Research) was used to record the droplet size and speed to validate the detector signal.

Off-the-shelf capacitive-to-digital converters (Analog Devices – AD7746) were used to extract the signal from the electrodes. A schematic of the detection system is shown in Fig. 4. The AD7746 microchip has built-in excitation sources and filtering/amplifying circuits in a 16-pin TSSOP configuration [35]. Using these commercially available converters significantly lowers the cost and provides a simple and scalable alternative to previously showed droplet detection systems [27,28]. A USB-powered microcontroller (Arduino Duemilanove ATmega328) was used to communicate with the AD7746. The microcontroller was programmed to output a real-time capacitance measurement signal which was displayed through a Labview interface.

The AD7746 provides two individual measurement channels with a 24-bit resolution. The full-scale linear (±0.01%) capacitance measurement range is ±4pF with a precision of 4fF. Measurement

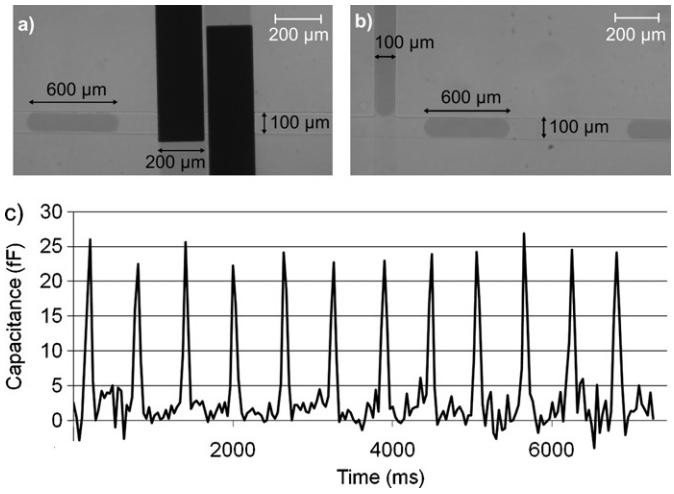


**Fig. 5.** Optical microscope image of (a) microchannel with coplanar electrodes and (b) T-junction droplet generator. (c) Measured capacitance signal with shown configuration.

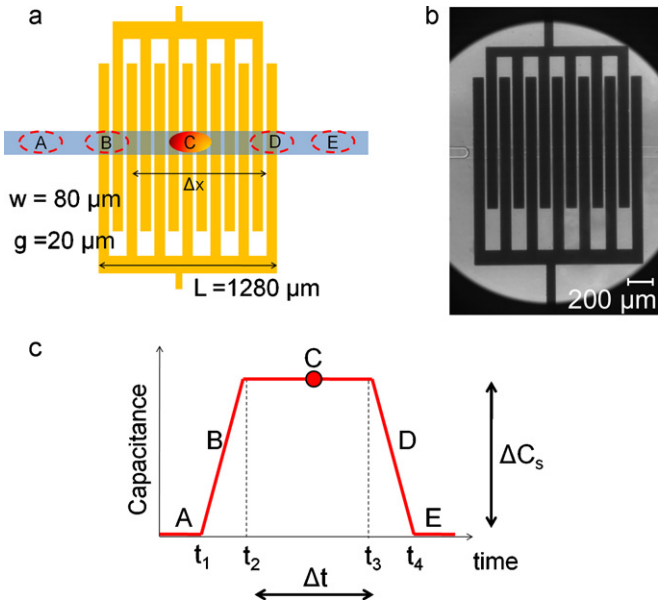


**Fig. 6.** (a) Schematic and (b) optical microscope image of droplet sensor with interdigital fingers. (c) Illustration of the ideal capacitance signal obtained from the interdigital sensor.

precision was validated using fixed capacitors. The electrical wiring to the microfluidic chip and the close proximity of the sensor electrodes may increase the baseline capacitance outside the specified range. This would cause an imprecision in the signal. To keep the measured signal within the high-accuracy linear measurement range, both channels are zeroed by tuning the internal offset capacitor during system start-up. The details of the offset calibration process can be found in the chip data sheet [35].

AD7746 has two measurement modes: single-ended and differential capacitance. In single-ended mode, two pins of AD7746 are used to make a two-prong capacitance measurement. For differential capacitance mode, three pins are used. One pin provides the excitation signal while other two pins are the sensing pins. The output signal is the difference of the two sensing signals. Both modes are utilized in this study as discussed in Section 4.3.2.

## 4. Experimental results and discussion

### 4.1. Detection of droplets

In this section we show that a two-prong sensor design can be used to detect the presence of droplets. In the next section, interdigital designs are used to also extract the droplet size and speed. Initial experiments of droplet detection were performed using sensors with two electrodes as shown in Fig. 5(a).

To determine the highest signal for capacitance change, multiple sensors with varying electrode widths (from 80 μm to 500 μm) were fabricated along a single microchannel. Electrode spacing was kept at 20 μm for all the designs. The measured capacitance change was between 15fF and 26fF. The analytical model suggests that increasing electrode width above the effective width does not increase the change in capacitance. Our experiments have shown that for a passivation layer of 2 μm, the detection signal saturates at 26fF whereas larger electrode widths slightly improve the detection signal. In Fig. 5, the measurements for 200 μm-wide electrodes are shown. For these measurements 600 μm-long droplets were used to cover the entire electrode region. Although identical droplets were used during the measurement, approximately 15% variation was observed in the impulse-like signals corresponding to droplets (Fig. 5(c)). This is due to the low sampling rate of the sensor.

For a 2 μm-thick passivation layer, the measured signals around 20fF agrees with the values predicted by the analytical model for a passivation layer thickness of 1–2 μm (Fig. 3). The thorough validation of the analytical model was not made due to the challenge of fabricating a thin uniform passivation layer. Toluene thinned PDMS was spin-coated on 1 in. × 3 in. microscope slides to form the passivation layer. When non-circular substrates are used, spin-coating from a pneumatic dispensing tip gives a coating thickness variation. Our attempts to make very thin conformal passivation layers failed due to the pits formed during baking. The thinnest passivation layer than can be made reliably was 2 μm.

### 4.2. Detection of droplet size and speed

Detection of droplet size and speed is achieved using interdigital electrodes as shown in Fig. 6. As a droplet first enters the sensing region ($t_1 < t < t_2$, state B), the capacitance signal increases, and then saturates once the droplet is completely in the sensing region ($t_2 < t < t_3$, state C), and then falls again when it leaves ($t_3 < t < t_4$, state D). The size of the droplet can be measured by the saturation signal, $\Delta C_s$. Larger droplets generate higher signals because they displace more oil within the sensing region. A limitation of this design is that droplets must be less than the length of the sensor or the signal will be completely saturated.

Speed can be detected using either the rise/fall time ($\Delta t = t_2 - t_1$) or the duration of the saturation state ($\Delta t = t_3 - t_2$). Our experiments indicated that the latter option provides better accuracy. The speed of a droplet is calculated using the formula $v = \Delta x/\Delta t$. $\Delta t$ is the saturation time and $\Delta x$ is the distance travelled by the droplet when it is completely in the sensing region. This distance can be calculated as

$$\Delta x = L_{sen.} - (L_{drop.} - h) \quad (7)$$

where $L_{sen.}$ is the length of the sensor, $L_{drop.}$ is the length of the droplet (front to back) and $h$ is the channel height. Channel height is subtracted from droplet length because the curved front and back end of the droplet do not contribute significantly to the capacitance change.

In an interdigital finger configuration, each inner electrode forms two semi-spherical sensing regions. Therefore, the effective width is calculated as $2 \times 41\ \mu m = 82\ \mu m$ for a 50 μm high channel when electrode fingers are separated by 20 μm. According to the experimental results discussed in Section 4.1, larger electrode

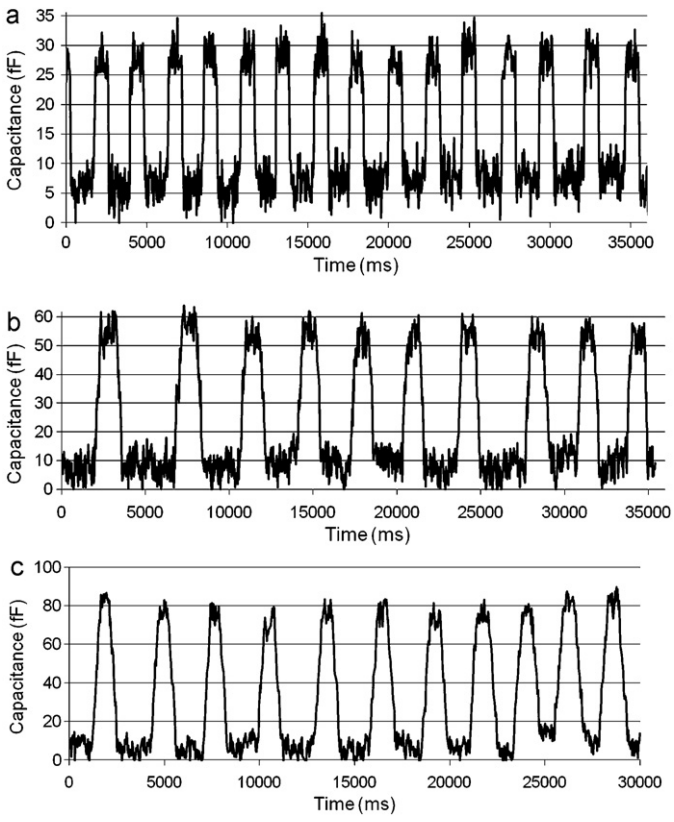


**Fig. 7.** Measured capacitance signal using interdigital electrodes shown in Fig. 6(b) for droplet sizes of (a) 250 μm, (b) 480 μm, and (c) 700 μm.

widths slightly improve the detection signal. However, for interdigital electrodes it is also important to keep the size of the sensor at minimum for three main reasons: (i) to reduce real-estate occupied by the sensor, (ii) to reduce the constraints on droplet spacing and (iii) to increase the number of sensing gaps which improves the smoothness of the signal.

To keep the sensor size as small as possible, we have used 80 μm-wide electrodes for the interdigital sensors. Droplet detection experiments were performed with droplets of varying size and speeds. First a calibration curve was obtained by correlating the change in capacitance ($\Delta C_s$) to the droplet size which was measured using the high speed camera. Three sample sensor signals are given in Fig. 7 for droplet sizes of 250 μm, 480 μm, 700 μm for the sensor design shown in Fig. 6(b). The saturation capacitance is directly proportional to the size of the droplets resulting in a linear calibration curve (Fig. 8).

Once an equation is found for droplet size, droplet speed can be measured using Eq. (7). The difference between the sensor results

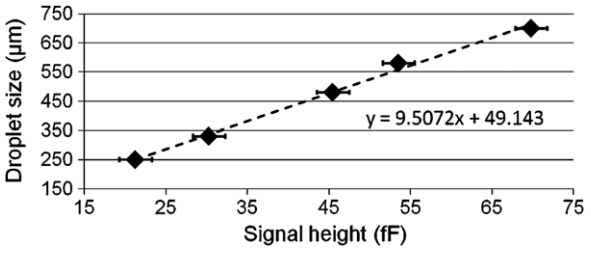


**Fig. 8.** Calibration curve showing a linear relationship between the capacitance signal change and the droplet size ($2a = 20$ μm, $w = 80$ μm, and $h = 50$ μm). Each point represents an average of 10 measurements. Error bars represent the minimum and maximum values. At steady-state, the system generates successive monodisperse droplets of negligible variation in size, therefore no error bars are seen on $y$-axis.

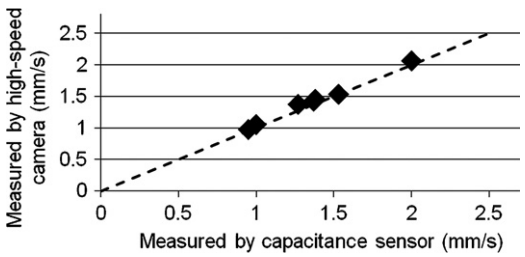


**Fig. 9.** Parity plot demonstrating the capacitive droplet speed measurements in comparison to measurements with high-speed camera.

and the measurements made using the high speed camera are summarized in a parity plot (Fig. 9). The capacitance sensor measurements are within 5% of the high speed camera results. The error is primarily caused by ripples in the saturation signal which makes it difficult to obtain precise readings of $t_2$ and $t_3$ (Fig. 6). Since the electrodes are fairly wide, the relative position of the droplet to the electrode center causes a slight change in the sensor reading, which leads to the ripples in the saturation signal.

### 4.3. Configuring capacitive sensors

AD7746 capacitance-to-digital converters are reconfigurable sensors designed for a variety of applications. The signal update rate (10–90 Hz), measurement mode (single-ended, differential) and excitation signal (2.7–5 V, 16–32 kHz) can be configured. In this section we discuss the maximum detection limit of the sensors, different measurement modes and scalability of capacitive sensing. Although specific parameters may be different for other commercial sensors, discussions in this section can be applied to any capacitor sensor and provides a guideline for sensor selection.

#### 4.3.1. Detection speed

Microdroplet based systems can generate droplets at kHz rate and therefore it is important to determine the maximum operating limits of the sensor for a given application. The output data rate ($freq_{samp.}$) of AD7746 can be changed between 10 Hz and 90 Hz with corresponding root mean square noise levels of 4.2aF and 40aF. Running the sensor at higher speeds compromises detection sensitivity. However, our experimental results show that water-in-oil droplets generate several tens of fF capacitance change, and therefore signal to noise ratio (SNR) is satisfactory even when the sensor is operated at 90 Hz.

For many applications, real-time droplet size and speed detection is very critical. Although the sensor can theoretically operate at 90 Hz, additional components in the system introduce delay times which reduce the effective rate of data display. We have evaluated the sensor performance by displaying the real-time signal either using a computer or an on-board LCD. When the sensor was set to 90 Hz, the effective rate of data display was measured as 30 Hz through the computer. Replacing the computer with an LCD yielded similar update rates. This shows that delay is due to the microcontroller rather than the display unit. Determining the effective update rate, we can calculate the detection limit of the system.

To evaluate the maximum limit of the sensors, we used the metric of the maximum number of droplets ($F_{max}$) that can be detected in a second (droplets/s). Detection of droplets requires sampling from both the continuous and dispersed phases. Assuming that coplanar electrodes are point detection sensors, sampling through the microfluidic channel is schematically shown in Fig. 10. For a system with constant droplet velocity, detection signals (shown as red circles) are taken with equal intervals. In order to detect droplets, at least one signal should be sampled from consecutive continuous and dispersed phases. The length of the segmented continuous

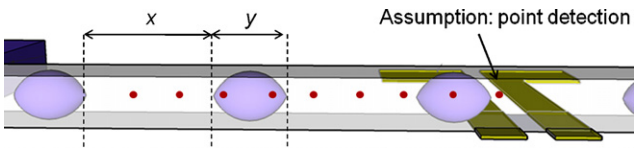


**Fig. 10.** Schematic of droplet detection used for throughput calculation.

and dispersed phases are denoted as $x$ and $y$ respectively. Then, the problem reduces to detect the minimum of $x$ and $y$. The equation for maximum detectable throughput can be written as

$$F_{\max} = \frac{freq_{samp.} \times \min(x, y)}{x + y} \quad (8)$$

To obtain the highest detectable throughput for a given system, the droplet length ($y$) and continuous fluid segment length ($x$) should be equal, which gives a maximum detection limit of $freq_{samp.}/2$. Therefore, the maximum theoretical detection throughput for our system is 30/2 = 15 droplets/s. During the experiments shown in this study, droplet generation frequency was lower than 5 Hz to stay well below the theoretical limit of 15 Hz. Using this result, the maximum detectable droplet velocity can be calculated. To illustrate, for a system with 100 μm-long droplets separated with 100 μm fluid segments, 200 μm × 15 droplets/s = 3 mm/s is the upper limit for detectable droplet velocity. For applications requiring higher droplet throughputs, faster sensors [29] or custom-made detection circuitries should be considered [27,36].

### 4.3.2. Detection mode

The commercial sensor chip can be configured to work in either single-ended or differential mode. When the sensor is configured in the differential mode, it uses three electrodes as shown in Fig. 11. One of the electrodes provides the excitation signal while the other two are set as sensing electrodes. The output signal is the difference between the two measured signals ($C_{output} = C_2 - C_1$).

A sample differential measurement is shown in Fig. 11(c) for 200 μm-long droplets using 80 μm wide electrodes. Each droplet gives a low and high signal couple as marked on the plot. This sensor can also be used for size or speed detection by measuring the time gap between sequential droplets or local minimum/maximum

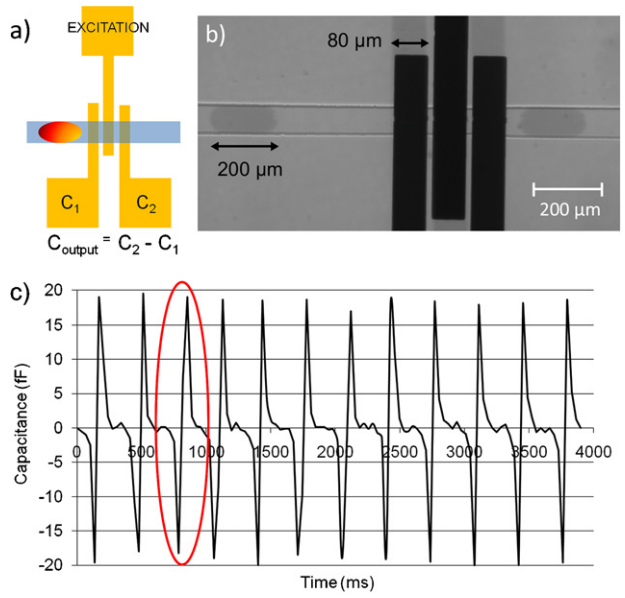


**Fig. 11.** (a) Schematic and (b) optical microscope image of differential droplet measurement sensor. (c) Measured capacitance signal. The corresponding up and down signals for a single droplet is marked.

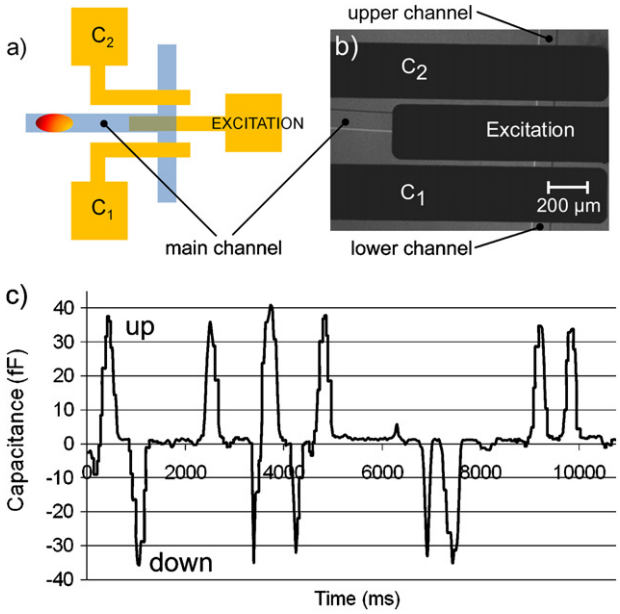


**Fig. 12.** (a) Schematic and (b) optical microscope image of differential droplet measurement sensor used at a T-junction. (c) Measured capacitance signal. The up and down peaks denote droplets going up and down at the T-junction. $C_{output} = C_2 - C_1$.

points. It is worth noting that a long and fast moving droplet and short and slow droplet would give similar signals, and therefore, the determination of size or speed requires *a priori* knowledge of the other parameter.

An interesting application for the differential measurement mode is to monitor droplet traffic at bifurcations [12,13]. If the electrodes are placed in parallel to the inlet channel as shown in Fig. 12(a) the output signal is an indication of the trajectory of the droplets (Fig. 12(c)). In this case a positive capacitance signal indicates a droplet taking the upper channel and a negative signal the lower channel ($C_{output} = C_2 - C_1$). Such a sensor configuration can be used to monitor droplet traffic in large networks with many bifurcations.

### 4.3.3. Scalability and cross-talk

The AD7746 has two independent channels for measurement on a single integrated circuit (IC). To demonstrate the use of multiple sensors a microdroplet sorting experiment is shown using a single bifurcation. Each channel is equipped with an interdigital sensor which is shown in Fig. 6(b) (denoted as triangles Fig. 13). Detection signals are displayed in real-time on separate plots. For each plot, two sliders are used for $x$- and $y$-axes. Sliders are adjusted manually by the operator to measure the saturation time ($x$-axis) and signal height ($y$-axis). A screen capture of the Labview interface during the experiments was recorded as a movie (refer to Supplementary file). As seen from the movie, all three sensors measure the same droplet length. The outlet pressures are kept at atmosphere pressure, so that two identical output branches have the same flow rates which are equal to the half of the inlet flow rate. This can be seen by the droplet speed measurements of the sensors. Sensor-1 is measuring a speed of 1.68 mm/s whereas sensor-2 and sensor-3 measure droplet speeds of 0.8 mm/s and 0.86 mm/s, respectively. For higher precision, the saturation time and signal height measurements can be automated through Labview.

When placing multiple sensors on a single device, care should be taken to reduce cross-coupling. To minimize the cross-talk between each sensor, the sensor trace width should be kept small and far away from each other. In this study, we have decreased the sensor trace width to 50 μm to decrease stray electric field lines. As well,

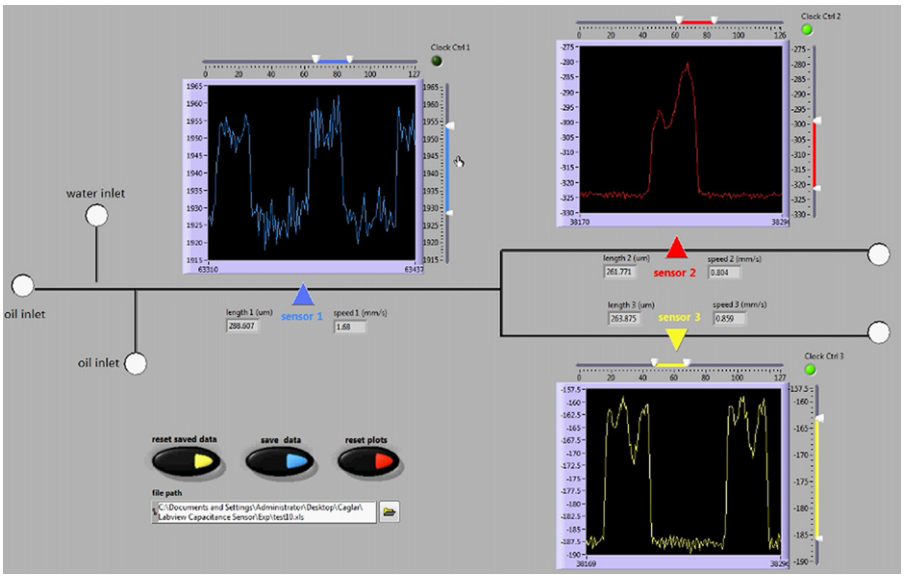


**Fig. 13.** Snapshot of Labview interface used to monitor droplet size and detection for a single T-junction network. Sensors are shown as triangles. Microdroplets are formed using a T-junction generator and the spacing is regulated with an additional continuous phase (oil) inlet. The Ca# of the system is kept low so that droplets move to the upper or lower branch at the T-junction without splitting (see Supplementary file for the screen captured movie of real-time detection).

external circuitry including connection wires should be shielded to reduce noise. The AD7746 ensures decoupling from its two internal channels. Adding an additional IC, which operates with the same frequency increases cross-coupling between the sensors. This problem can be solved by changing the excitation frequency on the second sensor from 32 kHz to 16 kHz. When the two ICs are set to different frequencies, they can automatically filter out the parasitic coupling signals with their internal circuitry. If the chip real-estate is populated with more sensors, ground traces can also be used to minimize the coupling [37].

## 5. Conclusion

We presented a scalable, inexpensive system for microdroplet detection in microfluidic devices which will widen the applicability of droplet based microfluidic devices. In this detection system, commercial capacitance sensors alleviate the need for detection circuitry design. Coplanar electrodes are used to form the sensor. An analytical model is presented to predict the detection signal considering the effects of the passivation layer and serve as a guideline for experimental design and experiments. For water-in-oil droplets, the capacitance change for each droplet is on the order of fF which is within the detection limit of most commercial capacitance sensors. Detection of droplet size and speed is demonstrated using interdigital electrodes. Different configurations of sensors as well as detection limit and scalability are presented.

## Acknowledgements

This work was supported by Natural Science and Engineering Research Council of Canada (NSERC) for research grants and Ontarios's Early Research Award to Dr. Carolyn Ren, research support to Dr. Caglar Elbuken and Canada Graduate Scholarship (CGS) to Tomasz Glawdel.

## Appendix A. Supplementary data

Supplementary data associated with this article can be found, in the online version, at doi:10.1016/j.sna.2011.07.007.

## References

[1] J.Q. Boedicker, L. Li, T.R. Kline, R.F. Ismagilov, Detecting bacteria and determining their susceptibility to antibiotics by stochastic confinement in nanoliter droplets using plug-based microfluidics, Lab Chip 8 (2008) 1265–1272.
[2] E. Brouzes, M. Medkova, N. Savenelli, D. Marran, M. Twardowski, J.B. Hutchison, J.M. Rothberg, D.R. Link, N. Perrimon, M.L. Samuels, Droplet microfluidic technology for single-cell high-throughput screening, Proc. Natl. Acad. Sci. U. S. A. 106 (2009) 14195–14200.
[3] J. Clausell-Tormos, D. Lieber, J.C. Baret, A. El-Harrak, O.J. Miller, L. Frenz, J. Blouwolff, K.J. Humphry, S. Koster, H. Duan, C. Holtze, D.A. Weitz, A.D. Griffiths, C.A. Merten, Droplet-based microfluidic platforms for the encapsulation and screening of mammalian cells and multicellular organisms, Chem. Biol. 15 (2008) 427–437.
[4] P.M. Gunther, F. Moller, T. Henkel, J.M. Kohler, G.A. Gross, Formation of monomeric and novolak azo dyes in nanofluid segments by use of a double injector chip reactor, Chem. Eng. Technol. 28 (2005) 520–527.
[5] D.K. Hwang, D. Dendukuri, P.S. Doyle, Microfluidic-based synthesis of non-spherical magnetic hydrogel microparticles, Lab Chip 8 (2008) 1640–1647.
[6] I. Shestopalov, J.D. Tice, R.F. Ismagilov, Multi-step synthesis of nanoparticles performed on millisecond time scale in a microfluidic droplet-based system, Lab Chip 4 (2004) 316–321.
[7] H. Song, D.L. Chen, R.F. Ismagilov, Reactions in droplet in microfluidic channels, Angew. Chem. 45 (2006) 7336–7356.
[8] M.J. Fuerstman, A. Lai, M.E. Thurlow, S.S. Shevkoplyas, H.A. Stone, G.M. Whitesides, The pressure drop along rectangular microchannels containing bubbles, Lab Chip 7 (2007) 1479–1489.
[9] O. Cybulski, P. Garstecki, Dynamic memory in a microfluidic system of droplets traveling through a simple network of microchannels, Lab Chip 10 (2010) 484–493.
[10] W. Engl, M. Roche, A. Colin, P. Panizza, A. Ajdari, Droplet traffic at a simple junction at low capillary numbers, Phys. Rev. Lett. 95 (2005) 4.
[11] M.J. Fuerstman, P. Garstecki, G.M. Whitesides, Coding/decoding and reversibility of droplet trains in microfluidic networks, Science 315 (2007) 828–832.
[12] M. Schindler, A. Ajdari, Droplet traffic in microfluidic networks: a simple model for understanding and designing, Phys. Rev. Lett. 100 (2008) 044501–044504.
[13] D.A. Sessoms, M. Belloul, W. Engl, M. Roche, L. Courbin, P. Panizza, Droplet motion in microfluidic networks: hydrodynamic interactions and pressure-drop measurements, Phys. Rev. E 80 (2009) 10.
[14] D.N. Adamson, D. Mustafi, J.X.J. Zhang, B. Zheng, R.F. Ismagilov, Production of arrays of chemically distinct nanolitre plugs via repeated splitting in microfluidic devices, Lab Chip 6 (2006) 1178–1186.
[15] N.T. Nguyen, S. Lassemono, F.A. Chollet, Optical detection for droplet size control in microfluidic droplet-based analysis systems, Sens. Actuators B: Chem. 117 (2006) 431–436.
[16] A.H. Tkaczyk, E.R. Tkaczyk, T.B. Norris, S. Takayama, Microfluidic droplet consistency monitoring and encapsulated cell detection via laser excitation, J. Mech. Med. Biol. 11 (2011) 1–14.
[17] S. Gawad, L. Schild, P. Renaud, Micromachined impedance spectroscopy flow cytometer for cell analysis and particle sizing, Lab Chip 1 (2001) 76–82.
[18] K. Cheung, S. Gawad, P. Renaud, Impedance spectroscopy flow cytometry: on-chip label-free cell differentiation, Cytometry A 65A (2005) 124–132.

[19] D. Holmes, J.K. She, P.L. Roach, H. Morgan, Bead-based immunoassays using a micro-chip flow cytometer, Lab Chip 7 (2007) 1048–1056.
[20] M.C. Cole, P.J.A. Kenis, Multiplexed electrical sensor arrays in microfluidic networks, Sens. Actuator B: Chem. 136 (2009) 350–358.
[21] C.X. Luo, X.J. Yang, O. Fu, M.H. Sun, Q. Ouyang, Y. Chen, H. Ji, Picoliter-volume aqueous droplets in oil: electrochemical detection and east electroporation, Electrophoresis 27 (2006) 1977–1983.
[22] N. Srivastava, M.A. Burns, Electronic drop sensing in microfluidic devices: automated operation of a nanoliter viscometer, Lab Chip 6 (2006) 744–751.
[23] F. Wang, M.A. Burns, Multiphase bioreaction microsystem with automated on-chip droplet operation, Lab Chip 10 (2010) 1308–1315.
[24] J.Z. Chen, A.A. Darhuber, S.M. Troian, S. Wagner, Capacitive sensing of droplets for microfluidic devices based on thermocapillary actuation, Lab Chip 4 (2004) 473–480.
[25] E. Ghafar-Zadeh, M. Sawan, D. Therriault, A 0.18-μm CMOS capacitive sensor lab-on-chip, Sens. Actuator A: Phys. 141 (2008) 454–462.
[26] J. Gong, C.J. Kim, All-electronic droplet generation on-chip with real-time feedback control for EWOD digital microfluidics, Lab Chip 8 (2008) 898–906.
[27] X.Z. Niu, M.Y. Zhang, S.L. Peng, W.J. Wen, P. Sheng, Real-time detection, control, and sorting of microfluidic droplets, Biomicrofluidics 1 (2007) 12.
[28] H. Ren, R.B. Fair, M.G. Pollack, Automated on-chip droplet dispensing with volume control by electro-wetting actuation and capacitance metering, Sens. Actuators B: Chem. 98 (2004) 319–327.
[29] S. Murali, X.G. Xia, A.V. Jagtiani, J. Carletta, J. Zhe, Capacitive Coulter counting: detection of metal wear particles in lubricant using a microfluidic device, Smart Mater. Struct. 18 (2009) 6.
[30] L.L. Sohn, O.A. Saleh, G.R. Facer, A.J. Beavis, R.S. Allan, D.A. Notterman, Capacitance cytometry: measuring biological cells one by one, Proc. Natl. Acad. Sci. U. S. A. 97 (2000) 10687–10690.
[31] A.V. Mamishev, K. Sundara-Rajan, F. Yang, Y.Q. Du, M. Zahn, Interdigital sensors and transducers, Proc. IEEE 92 (2004) 808–845.
[32] J.C. McDonald, D.C. Duffy, J.R. Anderson, D.T. Chiu, H. Wu, O.J. Schueller, G.M. Whitesides, Fabrication of microfluidic systems in poly(dimethylsiloxane), Electrophoresis 21 (2000) 27–40.
[33] R.F. Samy, Soft lithography for applications in microfluidic thermometry, isoelectric focusing, and micromixers, in: Mechanical Engineering, University of Waterloo, Waterloo, 2008, pp. 192.
[34] P. Garstecki, M.J. Fuerstman, H.A. Stone, G.M. Whitesides, Formation of droplets and bubbles in a microfluidic T-junction-scaling and mechanism of break-up, Lab Chip 6 (2006) 437–446.
[35] Analog Devices AD7746: 24-bit, 2 Channel Capacitance to Digital Converter, in, 2010.
[36] G.A. Ferrier, A.N. Hladio, D.J. Thomson, G.E. Bridges, M. Hedayatipoor, S. Olson, M.R. Freeman, Microfluidic electromanipulation with capacitive detection for the mechanical analysis of cells, Biomicrofluidics 2 (2008) 44102.
[37] Microchip AN1102 – Layout and physical design guidelines for capacitive sensing, in, 2007.

## Biographies

**Caglar Elbuken** received his B.Sc. degree in Electrical and Electronics Engineering from Bilkent University, Turkey in 2004 and his Ph.D. degree in Mechanical and Mechatronics Engineering from University of Waterloo, Canada in 2008. His research interests include microfluidics and MEMS with a focus on biological assays and detection systems.

**Tomasz Glawdel** received his B.A.Sc. in Mechanical Engineering from McMaster University, Canada in 2005 and his M.A.Sc. in Mechanical Engineering in 2008 from the University of Waterloo, Canada. He has continued at Waterloo pursuing a Ph.D. in Mechanical Engineering while holding an NSERC PGS D3 scholarship.

**Danny Chan** is a co-op student working at the Waterloo Microfluidics Lab. He is currently attending the University of Waterloo to obtain his undergraduate degree in Mechatronics Engineering and will be graduating in 2014.

**Carolyn L. Ren** received her Bachelor and Master's degrees from Harbin Institute of Technology (China) in 1992 and 1995, respectively. She received her Ph.D. from the University of Toronto in 2004 and joined the University of Waterloo afterwards. Dr. Ren's primary research interest is to develop microfluidic chip (Lab-on-a-Chip) technology for chemical and biomedical assays. She is currently a Canada Research Chair in Lab-on-a-chip technology.